# Global dayside ionospheric uplift and enhancement associated with interplanetary electric fields

Bruce Tsurutani,[1] Anthony Mannucci,[1] Byron Iijima,[1] Mangalathayil Ali Abdu,[2]
Jose Humberto A. Sobral,[2] Walter Gonzalez,[2] Fernando Guarnieri,[2] Toshitaka Tsuda,[3]
Akinori Saito,[4] Kiyohumi Yumoto,[5] Bela Fejer,[6] Timothy J. Fuller-Rowell,[7]
Janet Kozyra,[8] John C. Foster,[9] Anthea Coster,[9] and Vytenis M. Vasyliunas[10]

[1]   The interplanetary shock/electric field event of 5–6 November 2001 is analyzed using ACE interplanetary data. The consequential ionospheric effects are studied using GPS receiver data from the CHAMP and SAC-C satellites and altimeter data from the TOPEX/ Poseidon satellite. Data from ~100 ground-based GPS receivers as well as Brazilian Digisonde and Pacific sector magnetometer data are also used. The dawn-to-dusk interplanetary electric field was initially ~33 mV/m just after the forward shock (IMF $B_Z$ = −48 nT) and later reached a peak value of ~54 mV/m 1 hour and 40 min later ($B_Z$ = −78 nT). The electric field was ~45 mV/m ($B_Z$ = −65 nT) 2 hours after the shock. This electric field generated a magnetic storm of intensity $D_{ST}$ = −275 nT. The dayside satellite GPS receiver data plus ground-based GPS data indicate that the entire equatorial and midlatitude (up to ±50° magnetic latitude (MLAT)) dayside ionosphere was uplifted, significantly increasing the electron content (and densities) at altitudes greater than 430 km (CHAMP orbital altitude). This uplift peaked ~2 1/2 hours after the shock passage. The effect of the uplift on the ionospheric total electron content (TEC) lasted for 4 to 5 hours. Our hypothesis is that the interplanetary electric field "promptly penetrated" to the ionosphere, and the dayside plasma was convected (by $\mathbf{E} \times \mathbf{B}$) to higher altitudes. Plasma upward transport/convergence led to a ~55–60% increase in equatorial ionospheric TEC to values above ~430 km (at 1930 LT). This transport/convergence plus photoionization of atmospheric neutrals at lower altitudes caused a 21% TEC increase in equatorial ionospheric TEC at ~1400 LT (from ground-based measurements). During the intense electric field interval, there was a sharp plasma "shoulder" detected at midlatitudes by the GPS receiver and altimeter satellites. This shoulder moves equatorward from −54° to −37° MLAT during the development of the main phase of the magnetic storm. We presume this to be an ionospheric signature of the plasmapause and its motion. The total TEC increase of this shoulder is ~80%. Part of this increase may be due to a "superfountain effect." The dayside ionospheric TEC above ~430 km decreased to values ~45% lower than quiet day values 7 to 9 hours after the beginning of the electric field event. The total equatorial ionospheric TEC decrease was ~16%. This decrease occurred both at midlatitudes and at the equator. We presume that thermospheric winds and neutral composition changes produced by the storm-time Joule heating, disturbance dynamo electric fields, and electric fields at auroral and subauroral latitudes are responsible for these decreases.   INDEX TERMS: 2415 Ionosphere: Equatorial ionosphere; 2431 Ionosphere: Ionosphere/ magnetosphere interactions (2736); 2443 Ionosphere: Midlatitude ionosphere; 2435 Ionosphere: Ionospheric disturbances; 2134 Interplanetary Physics: Interplanetary magnetic fields; KEYWORDS: solar wind-ionosphere coupling, magnetosphere ionosphere coupling, magnetic storms, ionosphere

---

[1]Jet Propulsion Laboratory, Pasadena, California, USA.
[2]Instituto Nacional de Pesquisas Espaciais, São Paulo, Brazil.
[3]Research Institute for Sustainable Humanosphere, Kyoto University, Kyoto, Japan.
[4]Department of Geophysics, Kyoto University, Kyoto, Japan.
[5]Space Environment Research Center, Kyushu University, Fukuoka, Japan.

[6]Center for Atmospheric and Space Science, Utah State University, Logan, Utah, USA.
[7]Space Environment Center, Boulder, Colorado, USA.
[8]Department of Atmospheric, Oceanic, and Space Sciences, University of Michigan, Ann Arbor, Michigan, USA.
[9]Haystack Observatory, Massachusetts Institute of Technology, Westford, Massachusetts, USA.
[10]Max-Planck-Institut für Sonnensystemforschung, Katlenburg-Lindau, Germany.

## 1. Introduction

[2] Energy and momentum coupling between the interplanetary medium and the magnetosphere is well known. The interconnection between southward interplanetary magnetic fields (IMFs) and the Earth's magnetic fields leads to strong dawn-to-dusk electric fields and an overall increase in magnetospheric convection. This convection, in turn, causes intense ring current buildup and magnetic storms [*Gonzalez and Tsurutani*, 1987; *Gonzalez et al.*, 1994; *Kozyra et al.*, 1997; *Kamide et al.*, 1998]. However, these same dawn-to-dusk electric fields can have dramatic effects on the Earth's ionosphere. If the electric fields can penetrate to the ionosphere before "shielding" builds up [*Tanaka and Hirao*, 1973], they can modify equatorial ionospheric electrodynamics. Dawn-to-dusk directed electric fields will be eastward in the daytime and westward at night. Thus such electric fields will convect the ionosphere upward in the day and downward at night.

[3] Magnetospheric convection electric fields have another effect. The plasma sheet is convected Earthward forming a ring current, and a magnetic storm main phase commences [*Tsurutani and Gonzalez*, 1997]. This large increase in energy and momentum deposition in the high-latitude ionosphere and thermosphere causes a chain of events. The convection of ionospheric plasmas by these electric fields, through ion collisions with neutrals, leads to neutral winds with velocities in excess of 1 km/s. Joule dissipation within the high-latitude thermosphere drives large-scale wind surges. These winds alter the midlatitude ionosphere by moving plasma along field lines to regions of altered composition [*Proelss*, 1997; *Fuller-Rowell et al.*, 1997; *Buonsanto*, 1999]. The flow from high to low latitudes, through continuity, causes upwelling of the neutral gas and an increase of nitrogen molecules relative to oxygen atoms. This in turn leads to increased ion recombination rates and ionospheric plasma density reductions.

[4] It is the purpose of this paper to examine an interplanetary event with an unusually strong southward (negative $B_Z$ in GSM coordinates) interplanetary magnetic field to identify the ionospheric consequences throughout the magnetic storm. Ionospheric effects are wide-ranging in their manifestations, as described previously. At equatorial and midlatitude regions, one of the most outstanding modifications that can take place is to alter the ionospheric TEC (measured by dual-frequency GPS receivers). Little is presently known about the global-scale features of such modifications. Drastic changes in ionospheric vertical TEC can be produced by intense disturbance electric fields originating from the magnetosphere-ionosphere interaction. The disturbance electric fields at low latitudes have been identified as (1) prompt penetration zonal electric field often observed in the equatorial latitudes [*Sastri*, 1988; *Fejer and Scherliess*, 1995; *Abdu et al.*, 1995, 2003; *Sobral et al.*, 1997, 2001; *Sastri et al.*, 2002; *Kelley et al.*, 2003], following the early theoretical work of *Blanc and Richmond* [1980], and/or (2) delayed electric fields produced by the disturbance dynamo driven by Joule heating due to storm energy input at high latitudes [*Blanc and Richmond*, 1980;

*Richmond and Lu*, 2000; *Scherliess and Fejer*, 1997]. These latter electric fields, depending on their polarity and duration, could cause large uplifts or downdrafts of the ionospheric plasma leading to large-scale local time dependent enhancements or decreases of the vertical TEC. The effects at low latitudes are especially important because the equatorial plasma fountain is highly responsive to such disturbance electric fields and the latter can strongly affect space-based communications and GPS application systems. We will show that downdrafts of the ionosphere can lead to net TEC reductions and uplifts can lead to net TEC enhancements. Disturbance thermospheric winds associated with the disturbance dynamo processes could also cause significant modifications of the TEC at low and midlatitudes [*Fuller-Rowell et al.*, 1997]. In this paper we will address the interesting problem of the global-scale ionospheric response to an intense solar wind dawn-to-dusk electric field and related auroral zone and magnetic storm activities. The resulting equatorial disturbance electric field variations appear to control a major part of the observed global TEC features. Effects in both the storm main phase and recovery phase will be discussed. We will use satellite (CHAMP, SAC-C) GPS data, satellite altimeter (TOPEX) data, and ground-based GPS data, as well as Brazilian digital ionosonde data and magnetometer data from the Pacific sector in the analyses. The interplanetary event will be analyzed using ACE solar wind data.

## 2. Method of Analyses/Data Used

[5] The ACE satellite was upstream of the Earth at a GSM position of ($1.4 \times 10^6$ km, $1.2 \times 10^5$ km, $-2.0 \times 10^5$ km). In this coordinate system, $\hat{x}$ is in the direction from Earth to the Sun,

$$\hat{y} = \frac{\hat{x} \times \hat{M}}{|\hat{x} \times \hat{M}|},$$

where $\hat{M}$ is the north magnetic pole and $\hat{z}$ completes the right-hand system. The plasma detector and the magnetometer are described by *McComas et al.* [1998] and *Smith et al.* [1998], respectively. Owing to the contamination of energetic particles, the ACE SWEPAM plasma data are provided with reduced time resolution (R. Skoug, personal communication, 2003).

[6] Global Positioning System (GPS) satellite signals were received by both ground-based receivers (~100 distributed around the globe) and low-altitude satellites. A schematic of this is shown in Figure 1. There were 28 GPS satellites located in circular (Earth) orbit at an altitude of 20,200 km. For simplicity, only one GPS satellite is illustrated in the figure. Each receiver simultaneously tracked multiple GPS satellite signals. The phase delays in the dual frequency electromagnetic radio signals from the GPS satellites to the receivers are directly related to the enhanced index of refraction and the total number of electrons along the lines of sight.

[7] The CHAMP and SAC-C orbits around the Earth are shown in Figure 2. The satellite orbital parameters are given
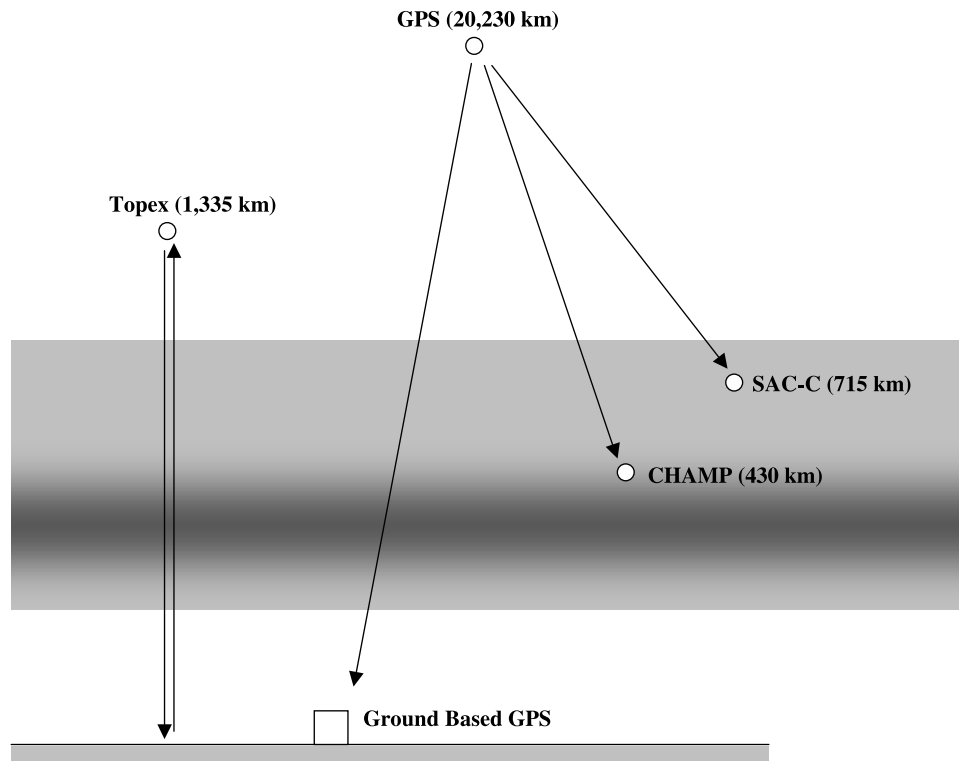
**Figure 1.** A schematic of GPS satellite and low-altitude satellite and ground-based GPS receivers. The TOPEX-Poseidon satellite carries an altimeter instrument. The system is used to measure multipoint ionospheric path-integral total electron content. The shaded area represents the ionosphere.

in Table 1. CHAMP was in a polar orbit (87° inclination) at an altitude of ∼430 km with an orbital period of 91 min. The CHAMP TEC data have been derived from the processing of dual frequency phase delay and pseudorange information. Data for elevation angles greater than 50° away from the vertical were not used. Otherwise, no other deletions have been performed. The TEC data have been "verticalized" assuming a spherical shell ionosphere of uniform (horizontally stratified) density 700 km thick above the CHAMP altitude.

[8] The SAC-C spacecraft orbit is also shown in Figure 2 and is described in Table 1. The SAC-C data were processed in a manner similar to that of CHAMP, except the ionosphere was modeled as a spherical shell of uniform electron density extending 2000 km above the SAC-C altitude.

[9] The TOPEX/Poseidon's dual frequency altimeter data are used to obtain downward viewing TEC information (See Figure 1 and Table 1). The TOPEX altimeter measures the vertical electron content beneath the satellite. Because this instrument is only used to measure ocean heights, there are data gaps over landmasses.

[10] The ground-based GPS data set used is composed of ∼100 stations from the International GPS Service data centers. The obliquity function used to estimate the vertical TEC is computed modeling the ionosphere as a spherical slab of uniform electron density between 450 and 650 km altitude. The latitude and longitude at which the ground-to-satellite line-of-sight intersects the ionosphere is computed using a spherical shell at 450 km altitude. Details concerning the removal of instrumental offsets for both ground-based receivers and satellite receivers is beyond this paper. If the reader is interested in further information on this topic, we refer him/her to *Mannucci et al.* [1998].

[11] At and in the immediate vicinity of the magnetic equator, the ionospheric vertical plasma drift is a direct measure of the zonal electric field. The vertical drift was obtained from vertical sounding Digisondes (digital ionosondes) operated at two equatorial sites, Sao Luiz (2.33°S, 44.2°W, dip angle: −0.5°) and Fortaleza (3.9°S, 38.45°W, dip angle: −9°), Brazil. The Digisondes provide, at 10 to 15 min resolution, the variation of the equatorial ionospheric height over a wide range of plasma frequencies (in the HF band). The rate of change of these heights as a function of time is a measure of the vertical plasma drift velocity. This technique is valid for nighttime conditions, when the layer height is above ∼300 km. At lower heights, the increasing dominance of chemical recombination over transport processes could introduce an apparent vertical drift [*Bittencourt and Abdu*, 1981]. Daytime disturbance zonal electric field intensities were inferred from equatorial electrojet Delta H response using ground-based magnetometer data from Pacific longitude sector stations Yap (9.3°N, 138.5°E, dip angle: −0.6°) and Guam (13.6°N, 144.9°E, dip angle: 9°).

## 3. Results

[12] The interplanetary event of 5–6 November 2001 is shown in Figure 3. The top six panels are interplanetary parameters taken by the ACE spacecraft located at $1.4 \times 10^6$ km upstream of the Earth. From top to bottom, the parameters are the solar wind speed, the proton temperature, the solar wind ram pressure, the proton density, the
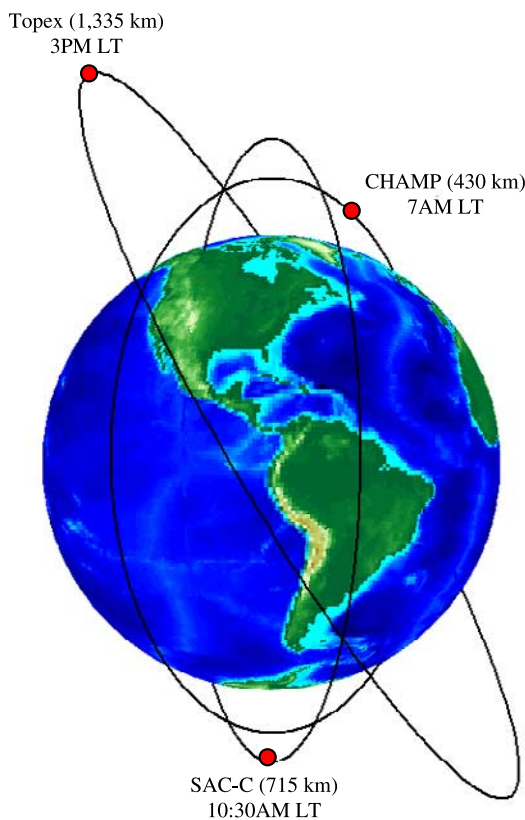
**Figure 2.** Satellite orbits about the Earth. This diagram illustrates the local time coverage of the three satellites used in this study.

magnetic field magnitude, and the magnetic field $B_Z$ component in GSM coordinates. Using the measured solar wind speed of $\sim$700 km/s, a convection delay time of $\sim$34 min from ACE to the magnetosphere was estimated. The solar wind data has therefore been shifted by this time in the figure to match the ground-based AE and Dst index data (the bottom two panels).

[13] The dashed vertical line labeled "C" indicates the start of a magnetic cloud [*Klein and Burlaga*, 1982]. The speed is $\sim$420 km/s and is thus a "slow" cloud (see *Tsurutani et al.* [2004] for discussion of slow cloud properties). It is identified by quiet magnetic fields with the general absence of large-amplitude Alfvén waves [*Tsurutani et al.*, 1988] and very low proton temperatures, $\sim$2.5 $\times$ $10^4$ K. The plasma density is $\sim$18 cm$^{-3}$ and $|B| \sim$ 18 nT.

[14] The solid vertical line labeled "S" is a fast forward shock. The shock occurred at $\sim$0120 UT at ACE. It is identified by an abrupt solar wind speed increase from $\sim$420 km/s to $\sim$700 km/s, a proton temperature increase to $\sim$8 $\times$ $10^5$ K, a density increase to $\sim$48 cm$^{-3}$, and a magnetic field increase to $\sim$70 nT. The magnetic field magnitude reached a maximum value of 80 nT $\sim$1 hour and 40 min after the shock passage.

[15] The high-speed stream event contains a small magnetic cloud from $\sim$1310 to 1630 UT. This is identified by the smooth magnetic fields, a proton density <1 cm$^{-3}$ and a temperature $\sim$2 $\times$ $10^4$ K. This cloud and its magnetic and electric fields are not important for the ionosphere effects focused on in this paper and will not be discussed further.

[16] The shock interaction with the upstream slow magnetic cloud has a profound effect on the resultant geomagnetic activity at Earth. The cloud has a steady $B_Z = -7$ nT (southward) field. The interplanetary shock compresses this preexisting interplanetary negative $B_Z$ [*Tsurutani et al.*, 1988] to $B_Z = -48$ nT. At the peak field strength, $\sim$1 hour 40 min after the shock, the $B_Z$ component reached $-78$ nT. Two hours after the shock, $B_Z$ was $\sim-65$ nT. $B_Z$ remained at negative values until $\sim$3+ hours after the shock. This long-duration, intensely negative IMF $B_Z$ feature is the cause of the main phase of the magnetic storm with $D_{ST} \cong -275$ nT. Such intense, long-duration IMF $B_Z$ events are always present during major magnetic storms [*Gonzalez and Tsurutani*, 1987; *Gonzalez et al.*, 1994].

[17] The sudden IMF negative $B_Z$ increase at the shock caused a sharp decrease in the Dst value. Dst reached a minimum value of $-275$ nT. There is also a substorm expansion phase onset just after the shock passage. This is noted in the increase in AE to $\sim$3000 nT. *Zhou and Tsurutani* [2001] and *Tsurutani and Zhou* [2003] have reported shock triggering of substorms and suggested that the onsets may be due to the shock ram compression effects or by the sudden onsets of large dawn-to-dusk cross-tail electric fields. For the remainder of the paper we will discuss the sudden intense interplanetary electric field at (and after) the shock and its effect on the Earth's ionosphere. This electric field onset occurs at $\sim$0120 UT at ACE and with a time shift of 34 min, it should have been imposed on the magnetosphere at $\sim$0154 UT. It should also be remembered that there is a small but important "precursor" interplanetary electric field associated with the negative $B_Z$ (due to the slow magnetic cloud ahead of the shock) and a concomitant moderate storm, occurring prior to the shock electric field event.

[18] Figure 4 shows the "verticalized" TEC above the polar orbiting CHAMP satellite for 2 days, 4 November 2001 (top panel) and 6 November 2001 (bottom panel). Since CHAMP has a nearly identical ground track every 2 days, we use the 4 November TEC data as a quiet "baseline" to compare with the 6 November response to the interplanetary shock. CHAMP was at a nearly constant altitude of $\sim$430 km and was at a nearly constant longitude at midlatitudes and at the equator during these 2 days. CHAMP crossed the equator at $\sim$0700 LT and at $\sim$1900 LT. The $\sim$1900 LT track is the one that is of interest for this paper. The time of the shock arrival at Earth is indicated by the vertical line labeled by an "S" in the bottom panel ($\sim$0154 UT).

[19] There are two important features to note in the figure. First, there is a major increase in TEC in the $\sim$1900 near-

**Table 1.** CHAMP, SAC-C, and TOPEX-Poseidon Satellite Orbital Parameters[a]

| Satellite | Altitude | Inclination | Orbital Period | Local Time Equatorial Crossings (6 November 2001) |
|---|---|---|---|---|
| CHAMP | 430 km | 87° | 91 min | 0700–1900 |
| SAC-C | 715 km | 98° | 99 min | 1030–2230 |
| TOPEX' | 1335 km | 66° | 112 min | 0300–1500 |

[a]The columns contains the altitudes, inclinations, orbital periods, and local time equatorial crossings for 6 November 2001.
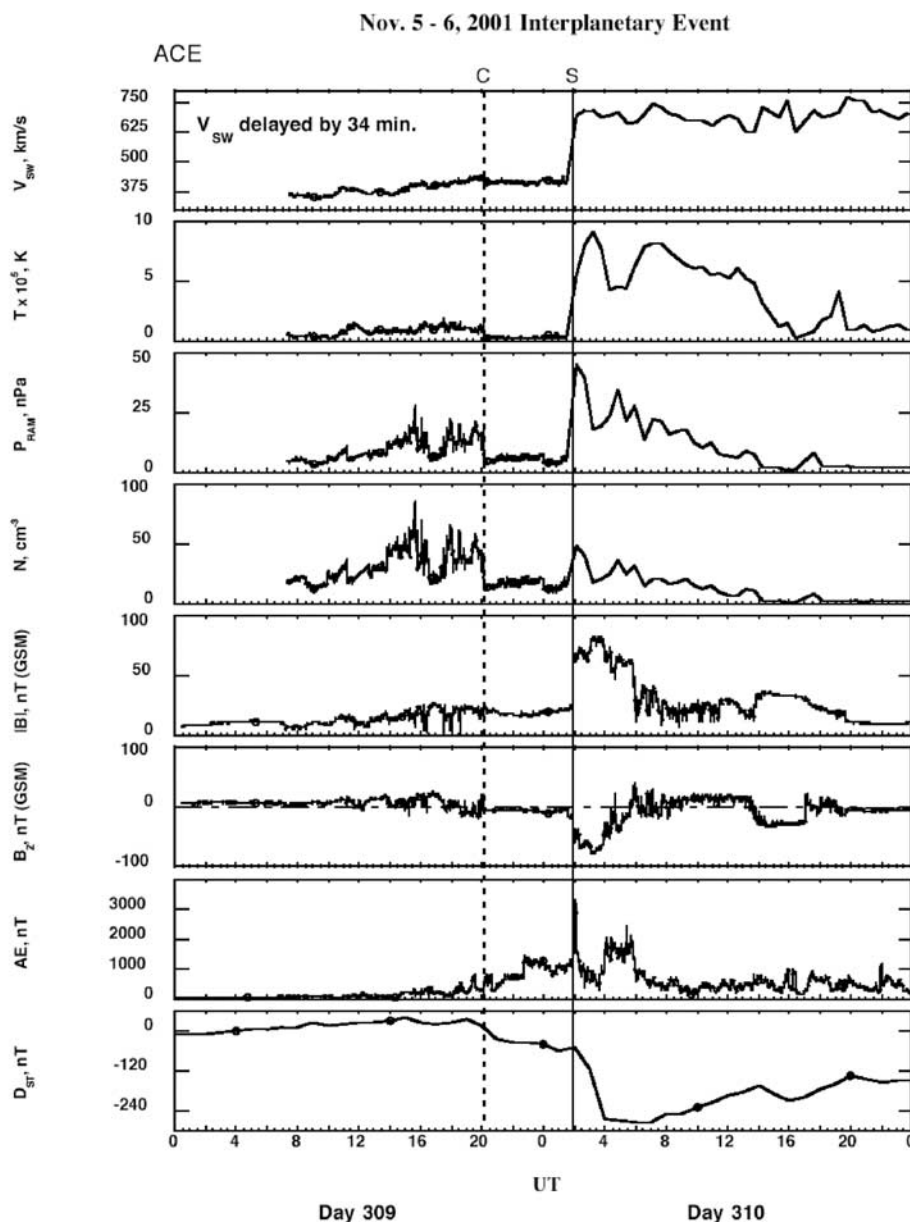
**Figure 3.** The interplanetary event of 5–6 November 2001. The interplanetary data is taken by the ACE spacecraft. The magnetic field is plotted in GSM coordinates. The time delay of the solar wind and magnetic field convection from ACE to the magnetopause is ∼34 min. Thus the interplanetary shock should impinge upon the magnetosphere at ∼0154 UT. A strong dawn-to-dusk electric field is imposed on the magnetosphere at this time. An AE ∼ 3000 nT substorm onset and a Dst = −275 nT magnetic storm onset also start at the time of the shock arrival.

equatorial crossing just after shock passage. At ∼0259 UT, the TEC is ∼125 TECU compared with ∼80 TECU over approximately the same landmass 2 days earlier (a TEC unit [TECU] is $10^{16}$ electrons/m²). On the next pass, the ionospheric electron enhancement above CHAMP is even larger. It is ∼160 TECU at ∼0425 UT, whereas it was ∼100 TECU 2 days earlier. Thus the TEC above 430 km at ∼1900 (dusk) increased by 55–60% some ∼2 1/2 hours after the shock. A second feature in the figure is a large decrease in the TEC above CHAMP well after the southward IMF $B_Z$ event (∼0154 to ∼0400 UT) had passed. The minimum TEC

value at the equatorial anomaly is 55 TECU at ∼1050 UT compared with ∼95 TECU on the quiet baseline day. The decrease is ∼45%. Another noticeable feature is the presence of only a single peak near the equator rather than the typical dual peak structure.

[20] Figure 5 shows the CHAMP ∼1900 LT verticalized TEC data in higher time resolution and plotted against magnetic latitude. (It should be noted that for such a plot, the time tick marks are different from panel to panel. This same format is used in Figures 6 and 7 as well.) The different plots in each panel correspond to successive
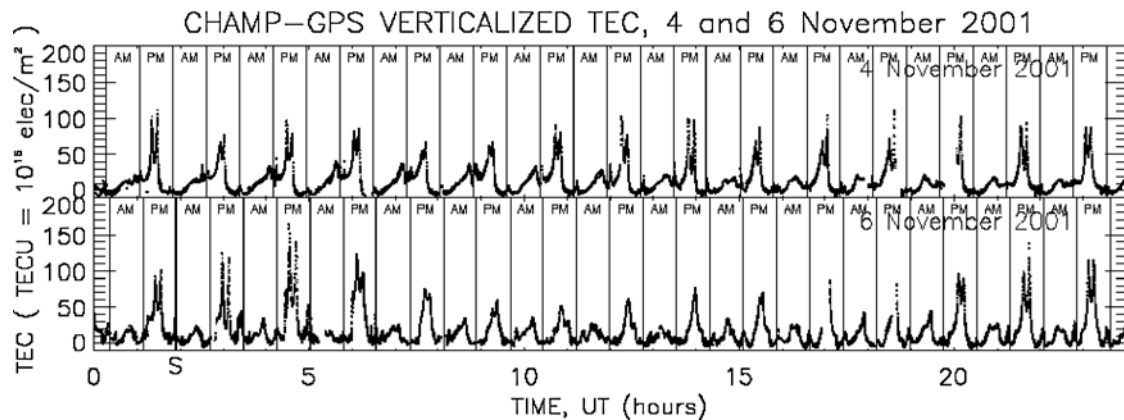
**Figure 4.** The CHAMP verticalized TEC data for 6 November 2001 and for a quiet day, 4 November 2001 (the latter for comparative purposes). The equatorial anomaly maxima at $\pm15°-20°$ increased by 55% to 60% within 3 hours after the shock passage at ~0154 UT 6 November. A substantial (~50%) decrease to values below quiet time levels occurs ~9 hours after the shock passage.

ascending GPS satellite tracks. The top panel (starting at 1856 UT) shows the two equatorial anomaly peaks located at $\pm15°-20°$ magnetic latitude (MLAT), with a local minimum (~40 TECU) at the magnetic equator (~1916 UT). After the shock, the TEC in the anomaly peaks increased (discussed in Figure 4) and the equatorial TEC decreased due to the enhanced fountain action induced by the disturbance eastward electric fields. At ~0300 UT, the equatorial TEC was 25 TECU compared with ~40 TECU at ~1916 UT. At ~0434 UT, the equatorial TEC increased to 50 TECU and then to 75 TECU by ~0608 UT, with the crests retreating toward the equator. With the anomaly peak intensities decreasing, the dual peak structure begins to disappear, which seems to mark the dominating role of a disturbance dynamo westward electric field. By ~0742 UT, there is just a single broad peak from $-20°$ to $+20°$ MLAT.

[21] Another interesting feature that can be noted in Figure 5 is the high electron densities at south latitudes well away from the equatorial region. Although the winter anomaly is known to affect the dayside peak $F$ region electron density, the TEC is expected to be larger in summer midlatitudes due to increased polar illumination. These densities drop off suddenly with higher latitudes. This "shoulder" is likely the signature of the plasmapause in TEC observations. One region can be noted at ~2030 UT, which is labeled with a "P." This occurs at a MLAT of $\sim-60°$. This "shoulder" in plasma density moves slowly to lower latitudes with increasing time. At ~0115 UT, it had moved equatorward to $\sim-54°$ MLAT (this slow inward motion may be associated with the "precursor" negative $B_Z$ prior to shock arrival). After the shock, this "shoulder" moves equatorward quite rapidly, reaching $\sim-43°$ MLAT by ~0425 UT. This movement of the plasmapause is associated with the expansion of magnetospheric convection to midlatitudes. Then the shoulder moves poleward once again and is at $\sim-47°$ at ~0732 UT. There is also very likely to be a longitudinal dependence developed in the location of the plasmapause due to the temporal and spatial variations in magnetospheric convection. It is also noted that the plasma content equatorward of the "shoulder" increases as the equatorward motion takes place. This will be discussed later.

[22] The exceptionally high electron densities at these midlatitudes can be noted at ~0425 UT and ~0559 UT. The TEC values are ~60–70 TECU at both of these times, in comparison with a value of ~20 TECU at ~0901 UT (not shown here). Thus the midlatitude TEC values are ~300+% greater than quiet time values.

[23] Figures 6a and 6b show the verticalized SAC-C GPS TEC data plots for 6 November. The measurements give the TEC at altitudes above ~715 km at ~1030 and ~2230 LT, respectively. Because of SAC-C's greater altitude, it detects far fewer electrons then does CHAMP. Note that in Figure 6a, time increases from right to left, and in Figure 6b, the opposite is true.

[24] Prior to the arrival of the shock on 6 November, the peak near-equatorial TEC was ~20 TECU. A broad, abrupt rise is noted at ~0300 UT to ~45–50 TECU, which seems to coincide in time with the equatorial ionospheric anomaly (EIA) trough depletion observed by CHAMP in the 1900 LT sector. By the next pass at ~0439 UT, the TEC had decreased to ~35 TECU. At ~0617 UT, the near-equatorial TEC was again ~20 TECU. The abrupt rise occurs just after the passage of the interplanetary shock. There is also a small midlatitude "shoulder" that is present at ~0604 UT. The "shoulder" is most prominent in the Southern Hemisphere and is present at $-37°$ MLAT at ~0604 UT (Figure 6b, 2230 LT). The decrease across the shoulder is from ~20 TECU to ~7 TECU.

[25] Figure 7 gives the downward looking TOPEX altimeter TEC data on 6 November. TOPEX was at an altitude of ~1335 km and was near the magnetic equator at ~1500 LT. The start of the data for each individual panel is on the right-hand side and time increases from right to left. TOPEX makes measurements only over the ocean, thus the presence of data gaps. However, extremely useful information is present in this data set. Prior to the arrival of the shock, at ~0154 UT, the equatorial anomaly peak had intensities of ~150 TECU. However, at ~0355 UT the northern anomaly had a maximum value of ~200 TECU at $+20°$ MLT (a ~33% increase). This EIA asymmetry seems to result from the prevailing quiet time interhemispheric (summer-to-winter) winds that cause larger increases of electron densities, mostly at heights near 430 km and below. By the next
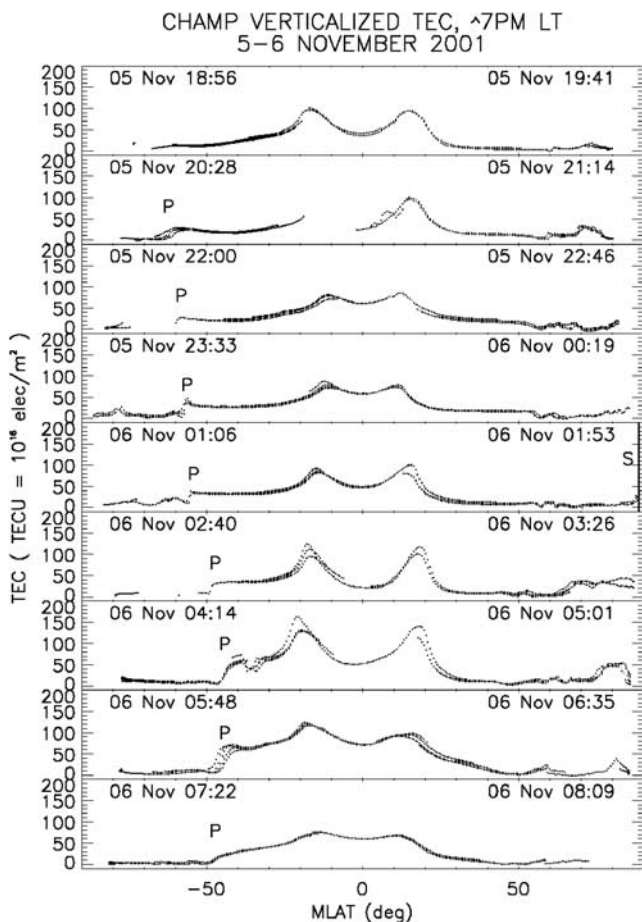
**Figure 5.** The CHAMP ~1900 LT verticalized TEC data plotted as a function of magnetic latitude. There are multiple plots in each panel; these correspond to multiple GPS satellites being tracked by the CHAMP receiver. Just after shock passage, the anomaly peaks become enhanced and the equatorial TEC becomes depressed. Later the equatorial TEC becomes ~55–60% greater than quiet time values, and the anomaly peaks diminish. In the bottom panel (~5 hours after shock passage), there is only a single peak extending from −20° to +20° MLAT. A second feature is a midlatitude "shoulder" in the electron density. It is labeled by a "P" for plasmapause. After shock passage, the "shoulder" moves rapidly equatorward from −57° to ~−43° MLAT and then poleward again.

dayside orbit (~0542 UT), the equatorial anomaly peaks became equal to each other with a value of ~180 TECU. The latitudinal separation of the two anomaly peaks had increased soon after the shock, similar to the effect observed in the CHAMP data. By ~0929 UT, the dual anomaly peaks disappeared and formed single a peak with a ~105 TECU amplitude.

[26] There is another feature present in the figure. There is a "shoulder" of TEC in the Southern Hemisphere. This can be noted in the third and fourth panels from the top. The TEC decreases from 85–90 TECU to 30–40 TECU at 45°–50° MLAT. The decrease is quite abrupt. The shoulder TEC values observed are 60–70 TECU by the upward viewing CHAMP satellite, ~20 TECU by upward

viewing SAC-C satellite, and 85–90 TECU by the TOPEX altimeter.

[27] Figure 8 shows the ground-based TEC data with satellite track TEC data superposed. The data is plotted as a function of local time and magnetic latitude. Figure 8a shows the 4 November 2001 "baseline" data from 0409 to 0456 UT. Figure 8b shows the 6 November 2001 shock event data from 0414 to 0500 UT (some 2 to 3 hours after the shock). Various satellite data (CHAMP upward GPS, SAC-C upward GPS, and TOPEX altimeter data) are also shown. The satellite data correspond to verticalized TEC above ~430 km at ~1900 (CHAMP), verticalized TEC above ~715 km at ~1030 (SAC-C), and TEC below ~1335 km at ~1500 (TOPEX). All satellite and ground GPS data are plotted to the same TEC scale.

[28] Figure 8a shows the enhanced TEC on the dayside due to solar UV irradiation of the ionosphere. It is centered at ~1400 LT and is slightly offset in latitude (~−10° MLAT). The center of the enhanced TEC intensities, the red area, extends from +20° MLAT to −30° MLAT. Such a latitudinal offset would be expected for northern wintertime (November) due to the influence of the prevailing circulation from south to north.

[29] Figure 8b shows a distribution with a remarkable contrast to that of Figure 8a. After the shock, the region of enhanced TEC over the Earth is much larger. The most obvious feature is the greater latitudinal extent, ranging from +50° MLAT to almost −50° MLAT. The westward and eastward extent of the red areas is approximately the same ~0900 to ~2100 LT.

[30] From a detailed comparison of Figures 8a and 8b at 1400 LT (the maximum) at the equatorial region, it is noted that on 6 November, the ground-based GPS has increased from ~145 TECU (4 November) to ~170–180 TECU. Thus there is an absolute increase in TEC at this local time by ~21%. Figures 8a and 8b also contain the CHAMP upward viewing TEC data (shown earlier in Figures 4 and 5). The TEC value above CHAMP is the same as that above the ground within an uncertainty of 10%. Thus at ~1900 LT the majority of the ionospheric plasma is above ~430 km altitude.

[31] Figure 9 is shown to illustrate the dayside TEC decrease. Figure 9a shows the baseline, 4 November 0848 to 0935 UT, and Figure 9b shows the postshock TEC data on 6 November from 0835 to 0939 UT. On 6 November the enhanced dayside TEC area (in red) is greatly diminished. The highest TEC values are confined quite close to the equator. The red areas are limited to ~±20° MLAT. At 1400 LT (maximum) at the equatorial region, the total ionospheric TEC shows a clear decrease. On 4 November the ground-based GPS value was ~155 TECU and this decreased to a value of ~130 TECU on 6 November. This is a ~16% absolute decrease.

[32] The TOPEX altimeter data shows good agreement between its values and those of the ground-based TEC measurements. In Figures 9a and 9b the color of the satellite measurements between 1400 and 1600 LT corresponds well to those made on the ground. In Figure 9a the transition from green to yellow occurs at ~−40° MLAT. In Figure 9b this occurs at ~−20° MLAT. Such equatorward motion of the transition region is consistent with high-latitude composition changes due to the summer-to-winter circulation
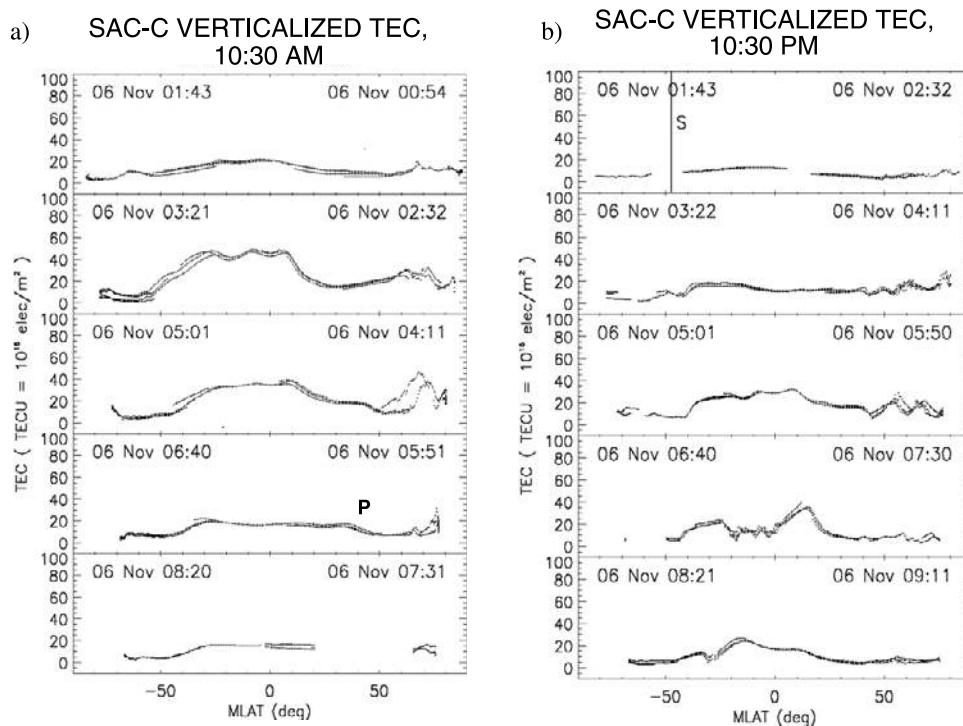
**Figure 6.** The TEC above SAC-C (~715 km altitude) at ~1030 LT plotted as a function of magnetic latitude. There is an abrupt rise in the near-equatorial TEC to ~45–50 TECU at ~0300 UT. This is a singular peak extending from −40° MLAT to +40° MLAT. By ~0528 UT, there is a clear plasma shoulder present at ~−37 MLAT. After the initial TEC increases, the feature decays and returns to normal by ~1000 UT (not shown). Figure 6b shows the SAC-C nighttime passes.

[*Fuller-Rowell et al.*, 1997]. A storm-time dynamo will enhance the equatorial motion. The increase in molecular species at midlatitudes in the summer hemisphere will deplete the ionosphere and move the contour equatorward. It is noted that this equatorward motion also occurs in the Northern Hemisphere. Thus the enhanced motion from high latitudes to lower latitudes is occurring there as well. This may imply that for this case, the magnetic storm energy deposition was so high that the induced thermospheric winds overcame the seasonal winds.

[33] In Figure 9b, there is a single equatorial peak in the TOPEX data at the equator (±10° MLAT) at 1400–1500 LT. This is similar to the CHAMP ~1900 LT results shown in Figure 5.

[34] The top two panels of Figure 10 show the height variations of the ionospheric F layer plasma frequencies obtained from ionosondes over two Brazilian equatorial stations during 5–6 November. The rate of change with time of these heights is a direct measure of the zonal electric fields. During the interplanetary shock event and consequential storm, Brazil was in the night sector. The top panel shows plasma frequency height variations over Sao Luis (2.33°S, 44.2°W, dip angle: −0.5°) and the middle panel shows those over Fortaleza (3.9°S, 38.45°W, dip angle: −9°).

[35] The bottom panel shows the equatorial electrojet (EEJ) current intensity over the Pacific equatorial station Yap (9.3°N, 138.5°E, dip angle: −0.6°), which was obtained by subtracting the diurnal range of the horizontal (northward) component of magnetic field intensity ($\Delta H$) over a non-EEJ station Guam (13.58°N, 144.87°E, dip

angle: 9°) from that of Yap. During the interplanetary shock event and consequential storm, Brazil was in the midnight sector and Yap was in the midday sector. A large decrease in the heights of isodensity lines starting near 0150 UT (2250 LT) marks the occurrence of a strong westward electric field associated with the shock in the midnight sector. The conspicuous height decrease that occurred in-phase at both Brazilian stations and its distinguishable magnitude with respect to the density isolines of 5 November identifies it as being caused by a disturbance westward electric field. The downward drift velocity obtained as dhF/dt is a significant underestimation of the true downward plasma drift due to the dominating role of the chemical recombination process as the height decreases below ~300 km. This was mentioned earlier. This point is evident from the decreasing slope of the isolines with decreasing height, starting at ~0150 UT, clearly seen over both the stations. The recombination drift is upward so that a downward electrodynamic drift (due to a westward electric field) can be perceived only if its magnitude exceeds that of the former. It can be shown that the positive slope region of the isolines (within the vertical lines 1 and 2) suggests apparent upward drifts at heights <300 km. In fact it corresponds to a downward plasma drift (of relatively smaller magnitude compared with the negative slope region in the beginning of this interval). Such results can be noted also in a recent case study over Jicamarca presented by *Fejer and Emmert* [2003]. When correction due to recombination is applied (as per *Bittencourt and Abdu* [1981]) the downward velocity which maximizes around 0245 UT corresponds to at least
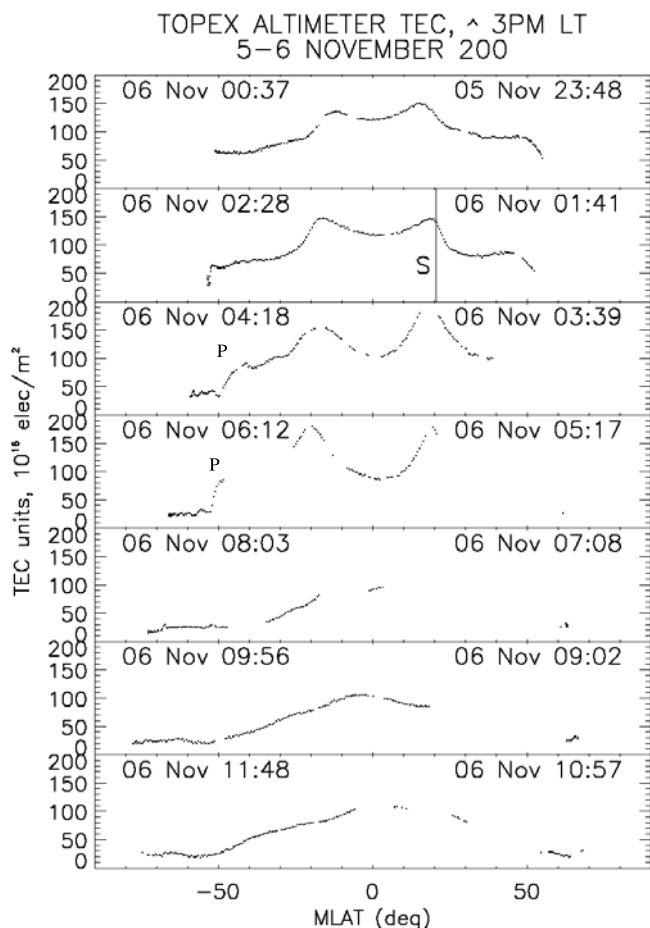
**Figure 7.** The TEC derived from the TOPEX altimeter, taken from an altitude of ~1335 km near a local time of ~1500 LT. The equatorial anomaly TEC increases from ~150 TECU before the shock to ~200 TECU in the pass after the shock. By ~0929 UT the dual anomaly peaks disappear and only a single equatorial peak is present. At ~0355 UT a TEC "shoulder" forms at ~−47° MLAT with a decrease from ~85−90 TECU at −45° MLAT to ~30−40 TECU at −50° MLAT.

100 m/s (that is, ~2 mV/m) over Fortaleza and ~80 m/s over Sao Luis. The possible cause of the different peak velocities over the two stations will be discussed separately. Additionally, there is a slight dissimilarity in the overall height variations between the two stations, which could be caused partly by the effect of meridional winds to which the ionosphere over Fortaleza, with larger magnetic dip angle, is more responsive than that over Sao Luis.

[36] The large increase of the EEJ intensity over the Pacific sector (bottom panel) is evidence for the very large disturbance penetration electric field of eastward polarity simultaneously produced on the dayside by the shock event. The maximum amplitude of the disturbance eastward electric field which corresponds to a maximum EEJ disturbance amplitude of ~150 nT coincides in time with the peak intensity of a westward disturbance electric field on the nightside. This westward (eastward) polarity of the penetration electric field on the nightside (dayside) is in general agreement with theoretical expectations and model

results [*Senior and Blanc*, 1984; *Spiro et al.*, 1988; *Fejer et al.*, 1990]. A schematic illustrating the interplanetary, magnetospheric, and ionospheric electric fields is given in Figure 11.

[37] Over Brazil, the electric field turns eastward at ~0340 UT and remains so until 0715 UT, when the polarity is westward over the Pacific. It should be noted that by ~0340 UT the dawn-to-dusk interplanetary electric field had already peaked and was beginning to decrease. The rather gradual developments of these electric fields both over Brazil and the Pacific suggest its source to be a combination of shielding electric fields and the disturbance dynamo (arising from enhanced geomagnetic activity before and after the shock encounter). What appears to be a reversal to westward electric fields over Brazil between ~0730 and 0830 UT (identified by the vertical lines 3 and 4) seems to be influenced by the sunrise occurring during this period. From ~0830 until ~1600 UT, the height variations over Brazil (the heights being generally less than during the same interval of the previous day) would suggest the presence of a westward disturbance dynamo electric field [*Abdu et al.*, 1997]. The corresponding disturbance dynamo electric field over the Pacific (night) sector is unclear from Figure 10 due to the absence of EEJ, although we expect an eastward polarity there.

## 4. Summary of Major Observations

[38] 1. An interplanetary shock, compressing upstream negative $B_Z$ interplanetary magnetic fields (IMF), caused an unusually intense interplanetary dawn-to-dusk electric field event. The southward (negative $B_Z$) IMF reached an intensity of $B_Z = -78$ nT 1 hour and 40 min after the shock. The intense southward IMF $B_Z$ lasted for over 3+ hours. Immediately after the arrival of the shock at the magnetopause, an AE = ~3000 nT substorm onset occurred. The onset of a great magnetic storm with intensity Dst = −275 nT was also a consequence of the intense, long-duration southward IMF event.

[39] 2. Large dayside TEC enhancements occurred immediately after shock passage and the imposition of the interplanetary dawn-to-dusk directed electric field. At ~1030 LT (SAC-C data), the TEC above ~715 km almost doubled from ~25−30 TECU to ~45−50 TECU within ~1/2 hours after shock passage. At ~1500 LT, the TEC below ~1335 km altitude increased from ~150 TECU to ~200 TECU within ~2 hours. At CHAMP there was an immediate increase from ~80 TECU to ~125 TECU after the shock. However, in the next pass at ~0425 UT (~2 hours 30 min after the shock), the peak intensity was higher still, ~160 TECU. The total (ground-based) equatorial ~1400 LT TEC increased from ~145 TECU to ~170−180 TECU within ~2 1/2 hours after shock passage. The dayside ionospheric TEC increases lasted from 2 to 3 hours after the shock.

[40] 3. The satellite observations of the near-equatorial region TEC indicate that strong ionospheric evolution occurred after the initial increase. TOPEX observations (at ~1500 LT) note first an asymmetry between the south and north anomalies (the north anomaly at +15° MLAT TEC is significantly larger), then an equalization, and then an evolution of the whole system to a single peak at the
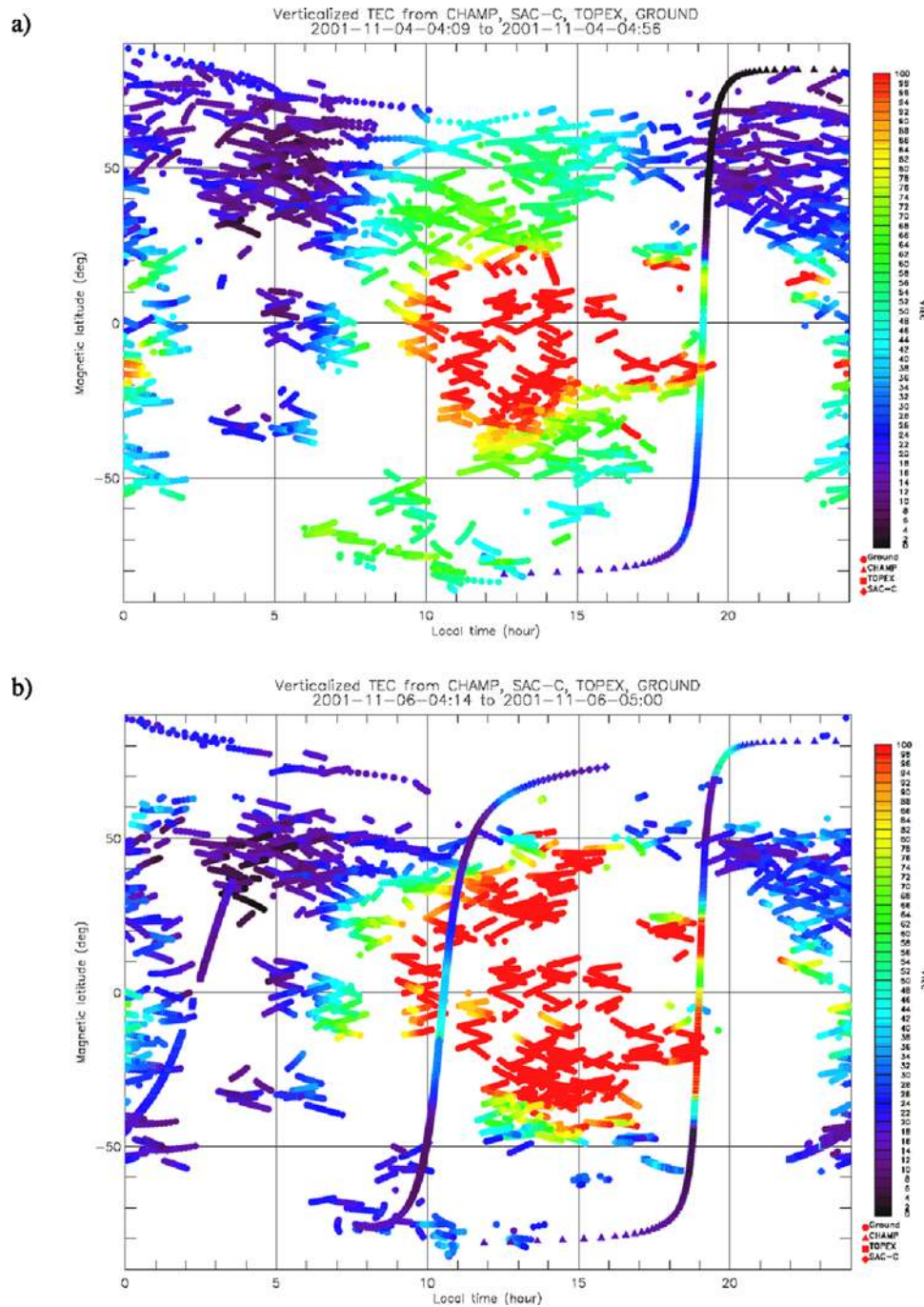
**Figure 8.** The ∼100-station ground-based TEC data for 4 November from 0409 to 0456 UT (background) in Figure 8a and for 6 November from 0414 to 0500 UT (post shock event) in Figure 8b. Various satellite TEC data are also shown (to the same intensity scale). The dayside postshock region of enhanced TEC is much broader in latitudinal extent, ranging from +50° MLAT to almost −50° MLAT.

magnetic equator. The electrons above SAC-C (>715 km) show a similar evolution. The TEC above SAC-C initially almost doubled to 45–50 TECU and then decayed to its normal values ∼8 hours after the initial rise.

[41]  4. Strong dayside ionospheric effects are detected at midlatitudes up to ±50° MLAT after the shock. Ground GPS data indicate that major global-scale plasma configuration changes occurred compared with quiet day conditions. "Shoulders" or sharp density drop-offs with increasing

latitude were noted in the TOPEX, SAC-C, and CHAMP data sets, as well as with ground GPS data. All satellites detected this feature only in the Southern Hemisphere. For the CHAMP TEC above ∼430 km, this "shoulder" moved from −54° MLAT at ∼0115 UT to −43° MLAT by ∼0425 UT and then moved poleward to ∼−47° by ∼0732 UT. The motion of the shoulder toward the equator occurred in the magnetic storm main phase, and the motion of the shoulder toward the poles occurred in the storm recovery phase. At 45° MLAT,
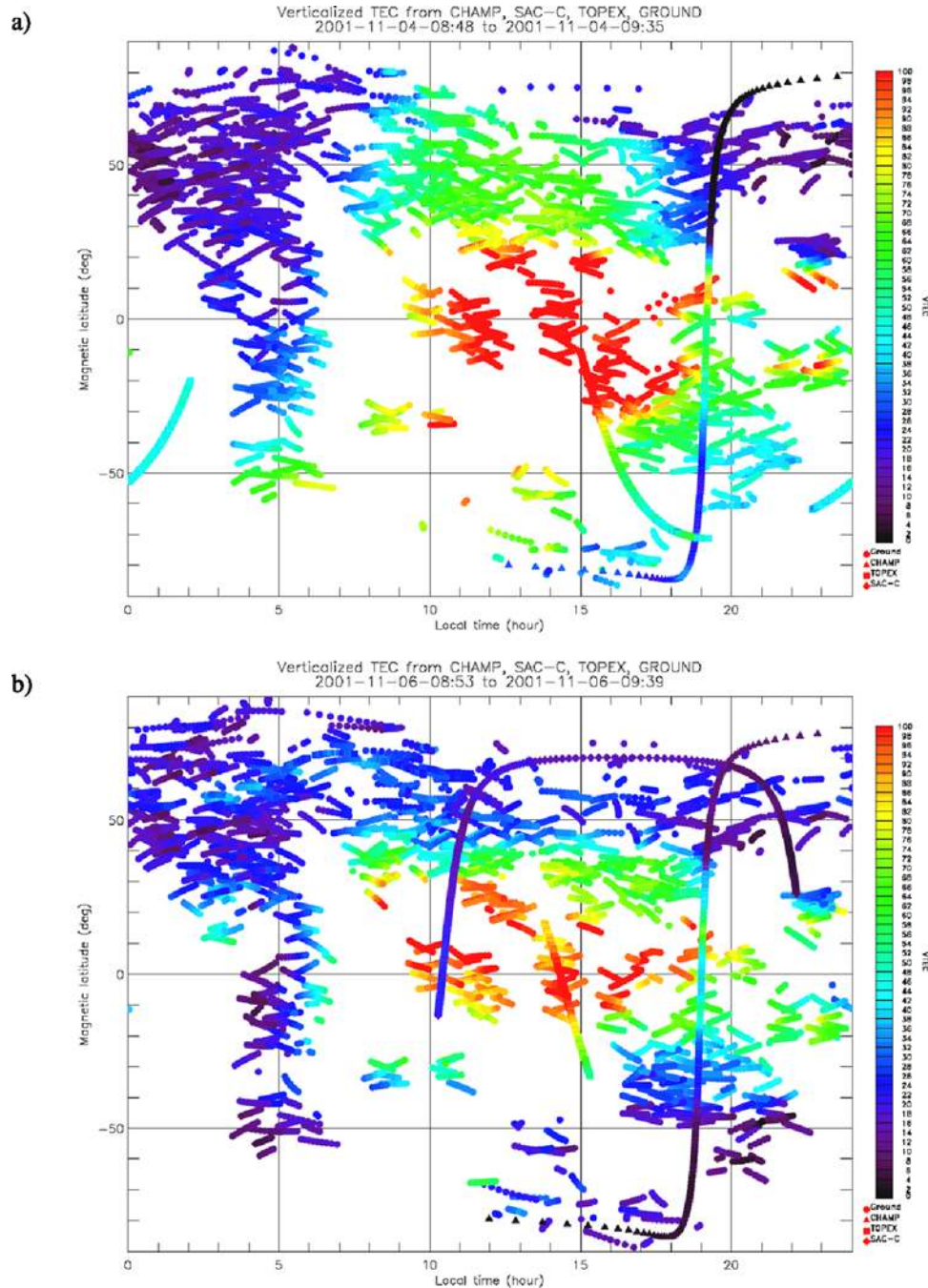
**Figure 9.** Ground-based GPS TEC and satellite receiver derived TEC for 0848 to 0935 UT, 4 November (Figure 9a) and for 0835 to 0939 UT, 6 November (Figure 9b). The dayside TEC is greatly reduced on 6 November. The highest electron column densities are reduced to a single peak within ±10° of the magnetic equator.

the ground-based TEC increased from ∼50 TECU to ∼90 TECU, an increase of ∼80%.

[42] 5. The nightside ionospheric effects were in many ways quite different from those of the dayside. After the shock passage, at the nighttime equator, there was a sharp downward motion of the nightside ionosphere due to a strong westward disturbance electric field lasting from 0200 to 0340 UT with simultaneous uplift of the dayside ionosphere due to a strong eastward electric field. This is due to the prompt penetration electric field (Figure 11). From ∼0340 to

∼0730 UT the nightside equatorial ionosphere (over Brazil) experienced a steady and strong eastward electric field lifting the ionosphere up to ∼600 km, as compared with the ∼300 km altitude for a "quiet" ionosphere of the previous day (shown in Figure 10). During the same interval, the dayside ionosphere (over the Pacific) experienced a westward electric field. From ∼0830 to 1600 UT a westward electric field (over Brazil) brought the ionospheric plasma to normal heights. This interval overlapped with the phase of the TEC decrease that follows the TEC enhancement phase.
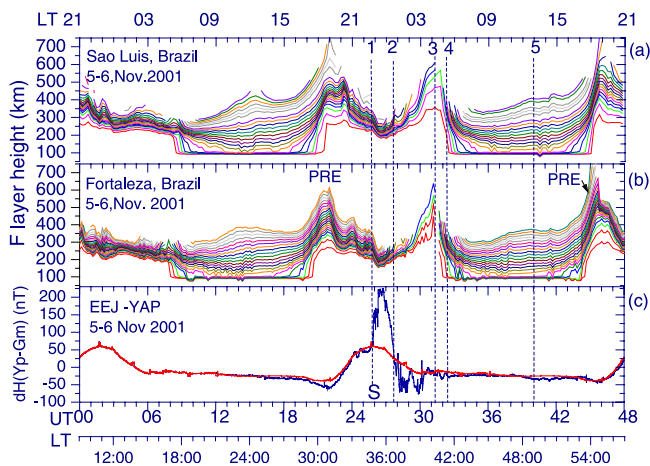
**Figure 10.** The height of the ionosphere (corresponding to electron plasma frequencies from 1 MHz and higher) over Sao Luis (a) and Fortaleza, Brazil (b). Brazil is in the evening sector. The equatorial electrojet (EEJ) current intensity over Yap in the midday sector is shown in Figure 10c. The reference day curve for Yap (in red) is taken from 5 November. The starting time in the figure is 0000 UT 5 November. The LT over Brazil (UT minus 3 hours) is shown at the top, and the LT at Yap (UT plus 9 hours) is shown at the bottom. The peaks in the F layer heights around 2100–2200 UT over Brazil are due to the prereversal eastward electric field enhancement (PRE) (marked in the figure). Vertical line 1 indicates the onset of the shock. The interval between lines 1 and 2 is the interval of strong westward prompt penetration electric field over Brazil in the midnight sector and simultaneous strong prompt penetration eastward electric field over Yap in the midday sector. The time interval 2–3 indicates an interval of eastward electric field over Brazil and westward electric field over Yap. The electric field polarity is uncertain during the interval 3–4 due to the sunrise effect. The interval 4–5 indicates westward electric field over Brazil (Yap does not show any effect due to the absence of the EEJ at night).

[43] 6. Well after the increase in the dayside TEC, there was a substantial dayside TEC decrease to values below quiet day values. This was best noted in the CHAMP dusk TEC values and by the ground-based dayside TEC plots. About 9 hours after the passage of the interplanetary shock, the CHAMP TEC value was ~55 TECU compared with ~95 TECU for a quiet day, or a ~45% decrease. Using a lower cutoff of ~95 TECU, the ground-based latitudinal range was +20° MLAT to −35° MLAT during quiet days, compared with +15° MLAT to −15° MLAT, ~9 hours after the shock. The ground-based TEC at 1400 LT at the equatorial region decreased from ~155 TECU to ~130 TECU.

## 5. Interpretation of Major Observations

[44] Since the observations were quite detailed and there were a variety of topics, we will attempt to give interpretations/conclusions only to the major points. In doing so, we will follow the outline of the summary section.

[45] 1. The interplanetary electric field was initially ~33 mV/m immediately after the shock and reached a value of ~54 mV/m 1 hour and 40 min later. The southward IMF event lasted ~3+ hours. A schematic of the interplanetary, magnetospheric, and ionospheric electric fields is shown in Figure 11. The penetration of the unusually strong interplanetary electric field into the magnetosphere caused the great magnetic storm main phase (Dst = −275 nT). The dawn-to-dusk directed electric field convected the plasma sheet into the magnetosphere, forming the storm-time ring current. The prompt penetration of the interplanetary electric field to both the nightside and dayside ionospheres had the strong effects that are the major focus of this paper. Figure 12 shows a schematic of a mechanism to increase the dayside TEC values. On the dayside, the dawn-to-dusk electric field will be eastward in direction, and the $\mathbf{E} \times \mathbf{B}$ plasma drift associated with this eastward electric field will lift the ionospheric plasma up to higher altitudes, above the CHAMP satellite and partially above SAC-C, regions where recombination rates are low. Solar UV radiation will form new electron-ion pairs at lower altitudes, thus leading to an overall dayside ionospheric TEC increase (noted in the TOPEX altimeter data). This same dawn-to-dusk electric field will be westward at night. This caused the strong downward plasma drift detected in the midnight sector over Brazil with concomitant recombination and TEC decreases. In fact, the westward electric field was significantly more intense than is apparent in the downward layer displacement rate (dhF/dt) if one considers recombination processes, which dominate at these heights.

[46] 2. CHAMP observed large TEC increases in the dusk sector, as did SAC-C and TOPEX in the forenoon and afternoon sectors, respectively. Thus it looks clear that the "daytime" TEC enhancement extends at least to the 1900 LT sector. Part of the cause of such a dusk increase of the TEC could possibly be the eastward convection of the enhanced daytime TEC. It looks more likely, however, that the dusk increase of the TEC could result from longitudinal extension to the dusk sector of the large dayside disturbance eastward electric field. We have noted earlier that the electric field intensity as inferred from the increased depth of the EIA crest intensity (in Figure 5) observed by CHAMP occurred at ~0300 UT, which is around the same UT of the peak eastward disturbance electric field as judged from the disturbance EEJ intensity over Yap and the maximum westward electric field over Brazil (Figure 10).

[47] 3. On the basis of the shock associated event sequences of Figure 3 and the observed dayside and nightside zonal electric fields of Figure 10, the evolution of the dayside and eveningside TEC can be explained as follows: after the shock passage and the imposition of the interplanetary electric field (with the associated AE activity enhancement of ~3000 nT), large eastward electric fields were present over the dayside with simultaneous large westward electric fields over the Brazilian night sector. The eastward electric field was responsible for the uplift of the dayside (and evening sector) ionosphere that contributed, due to the reduced loss rate of the elevated ionosphere and the presence of the ongoing ion production by solar radiation, to the large-scale buildup of the TEC over the dayside hemisphere seen in all the data sets. A schematic of this is shown in Figure 12. A decrease in the eastward
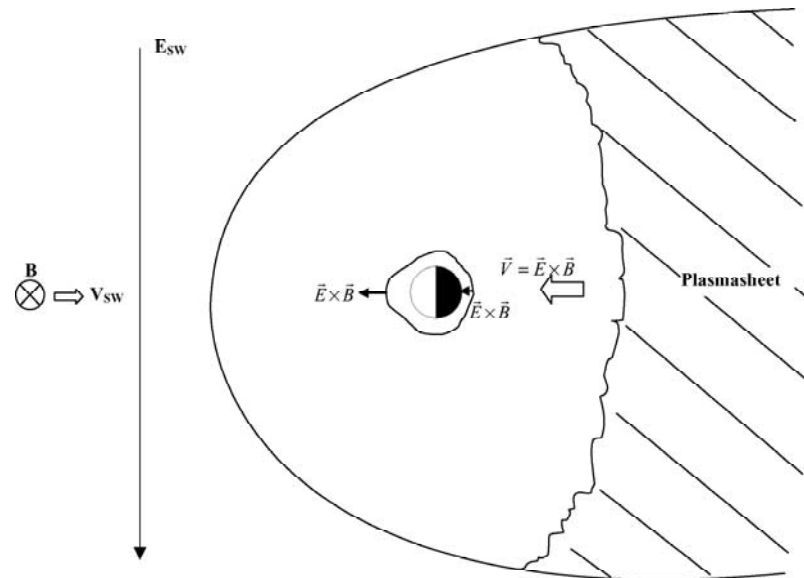
**Figure 11.** A schematic of electric fields in the solar wind and effects of penetrating fields in the magnetosphere and the nightside and dayside ionospheres. A dawn-to-dusk directed interplanetary electric field is caused by the solar wind convection of southwardly directed interplanetary magnetic fields past the magnetosphere. Portions of this electric field penetrate into the magnetosphere and the ionosphere, causing strong $\mathbf{E} \times \mathbf{B}$ convection effects in both regions.
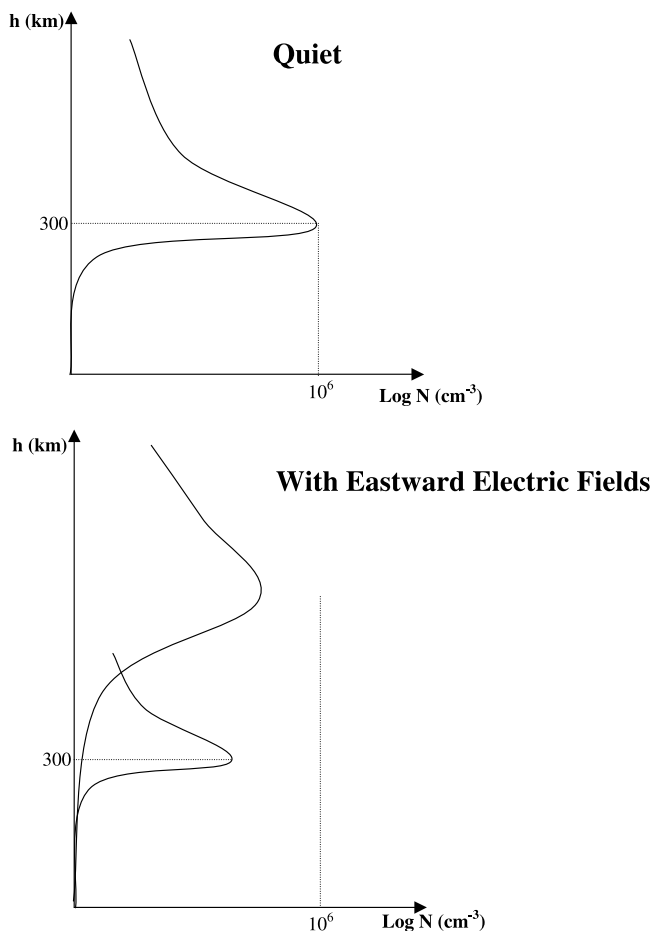
electric field, or even its subsequent possible reversal to westward, will not produce a prompt (immediate) decrease of the TEC due to the very slow F layer plasma decay rate by chemical recombination and the continuing ionization production by the solar radiation (even in the 1900 LT sector where ionization by direct solar radiation cannot operate, the TEC decay time should be of the order of hours). In other words, since the initial uplift of the dayside ionosphere by the prompt penetration eastward electric field lasted until ~0400 UT, the continuing TEC enhancement at 0500 UT in Figure 6b would point to the very slow decay of the uplifted/enhanced F layer ionization coupled with the competing effects from the prompt penetration eastward electric field from the 0330 UT AE enhancement and a developing disturbance dynamo westward electric field that set in around this time. The disturbance dynamo electric field is manifested by the rather gradual development of the large eastward electric field during 0300–0700 UT (indicated by the uplift of the postmidnight ionosphere over Brazil), with simultaneous westward electric fields in the afternoon Pacific sector (Figure 10). The westward polarity electric field seems to have contributed to reduce the eastward electric field intensity (attributed to the AE increase just mentioned before) to a greater degree in the afternoon sector than at 1900 LT (on the other hand, an expected westward polarity prompt penetration electric field in the postmidnight sector due to the 0330 UT AE enhancement should have diminished the intensity of the disturbance dynamo eastward electric field that prevailed over Brazil). By ~0600 UT, the AE activity shows recovery (Figure 3), which must have produced equatorward penetrating electric field of westward polarity on the day sector (according to the convection model results just mentioned above), which is added to the already present westward disturbance dynamo electric field in that sector, thus mark-ing the beginning of the TEC decrease over the equatorial region seen in all the data sets. The persistence of the disturbance dynamo westward electric field seems to be the driving force for the reduced/inhibited EIA that ensued in the following hours.

[48]  4. The initial asymmetries between the north ($+15°$ MLAT) and south ($-15°$ MLAT) equatorial anomalies caused by the shock electric field are quite strong, which seems to arise from the superposition of the strong disturbance eastward electric field effect on an already asymmetric EIA due to the interhemispheric circulation system characteristic of this season (that is, transequatorial and summer-to-winter hemisphere winds). This asymmetric situation seems to be disrupted by the action (possibly) of strong disturbance equatorward winds that followed. The nearly symmetric EIA peaks that followed might indicate an asymmetric forcing by the disturbance winds due to asymmetric energy input at north and south auroral regions.

[49]  5. Another new feature is that the dayside ionospheric TEC increases extended to $\pm 50°$ MLAT. The increases at these latitudes are ~80% greater than the quiet time values. One obvious possibility is that the prompt electric field not only affects the equatorial ionosphere but midlatitude regions as well. The "superfountain effect" (Figure 13) will also transport electrons from lower to higher magnetic latitudes.

[50]  The "shoulders" or plasma boundaries at $-54°$ MLAT (and more equatorward) are a dayside feature that has never been noted before. The equatorward motion of this boundary during the main phase of the magnetic storm is analogous to the inward motion of plasmaspheric magnetic field lines. The retreat of this boundary towards the pole is analogous to the expansion of the plasmasphere in the storm recovery phase. Similar results have been observed recently by the Radio Plasma Imager (RPI) on board the

values for the equatorial region ~1400 LT peak is a decrease of ~16%. This decrease is almost as impressive as the increase. The coexistence of both positive and negative storm phases in TEC has been previously noted by *Lu et al.* [2001]. The most likely explanation for the depletions in TEC at midlatitudes is neutral compositional changes [*Proelss*, 1997; *Fuller-Rowell et al.*, 1997; *Buonsanto*, 1999]. At lower latitudes, the long-lived depletions can be driven by the disturbance dynamo electric fields [*Blanc and Richmond*, 1980; *Scherliess and Fejer*, 1997; *Fuller-Rowell et al.*, 2002].

## 6. Comments

[53] The dawn-dusk interplanetary electric field has been invoked to cause a myriad of effects: (1) convection of the plasma sheet Earthward to create the ring current and the storm main phase, (2) uplifting of the dayside equatorial and midlatitude ionosphere and suppression of the nightside

**Figure 12.** A schematic of a proposed mechanism to increase the dayside total electron content (TEC). The top panel shows the dayside electron density profile during a quiet day. During promptly penetrating electric field intervals (lower panel), an eastwardly (dawn-to-dusk) directed field will $\mathbf{E} \times \mathbf{B}$ convect the ionosphere upward where the recombination rate is low. Photoionization of the lower $F$ region neutrals produces new plasma, which replaces the uplifted plasma, leading to an overall increase in ionospheric TEC.

IMAGE satellite [*Reinisch et al.*, 2004]. It will be interesting to make a detailed comparison of this ionospheric data to IMAGE results for the same event to determine if plasmaspheric erosion (and the plasmapause) can be identified by ionospheric TEC data.
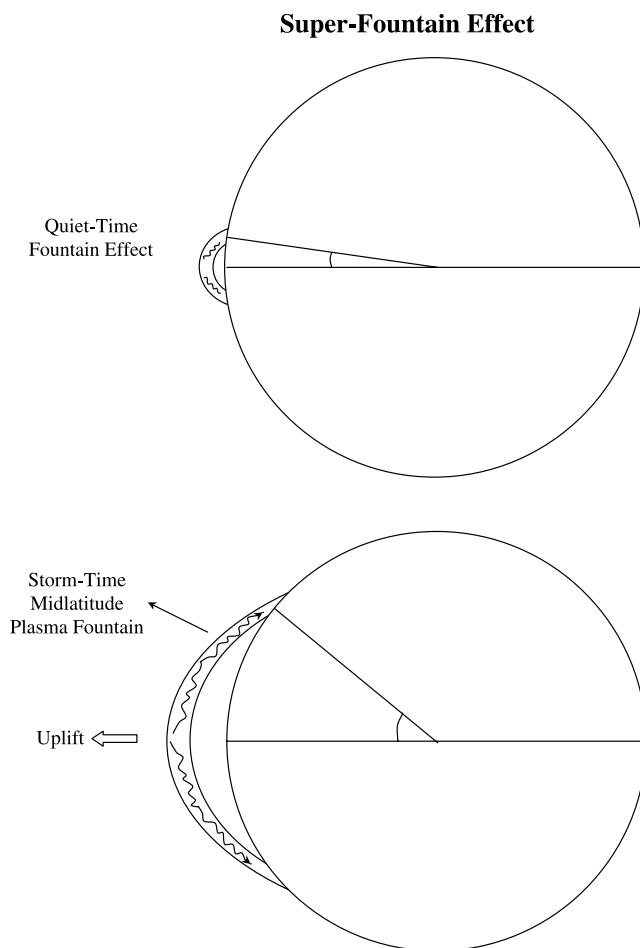
[51] It is also noted that the TEC measured at CHAMP altitudes increases as the "shoulder" or plasmapause moves equatorward. Transport of equatorial plasma to higher magnetic latitudes by the superfountain effect and plasmaspheric compression due to enhanced electric fields are possible mechanisms. It should be noted that possible indications of a superfountain effect like presented here may have been noted during the great storm of March 1989. A TEC depletion at the equatorial anomaly crest location [*Batista et al.*, 1991] was accompanied by concurrent large enhancements at higher magnetic latitudes [*Abdu*, 1997].

[52] 6. The CHAMP dayside ionosphere TEC decreases (~45%) well after the storm main phase. The ground-based



**Figure 13.** A schematic of a "superfountain effect," which may explain plasma enhancements at midlatitudes. The quiet time fountain effect is illustrated in the top panel. Uplift of equatorial plasma is followed by flow along magnetic field lines, leading to enhanced densities at ~±15° MLAT. In cases of extremely strong uplift during intense storm-time eastward electric fields, the spread of plasma will reach midlatitudes.

equatorial ionosphere, and (3) convection of the auroral zone ionospheric plasmas such that ion-neutral collisions form thermospheric winds that propagate to low latitudes.

[54]  The intense electric fields strongly affect the dayside midlatitude ionospheric plasma densities. The abnormally high TEC values, when eroded away by the magnetospheric convection electric fields, led to a sharp "shoulder" indicative of the plasmapause. Such signature may be also present (but less noticeable) during smaller magnetic storm events, and thus GPS data might provide another tool to identify plasmaspheric erosion events and a measure of magnetospheric convection electric fields. At this time we do not know how this GPS signature is related to Subauroral Polarization Streams (SAPS) [*Foster and Vo*, 2002; *Foster et al.*, 2002]. Also we remain with the question "why does the plasmapause signature occur in only one hemisphere"?

[55]  Enhanced seasonal winds could have caused the Southern Hemispherical TEC decrease that occurred well after the magnetic storm. However, it was noted that the decrease was more-or-less symmetric, occurring both in the dayside Northern Hemisphere and also the dayside Southern Hemisphere. Was the storm-time precipitation so intense that it "overpowered" seasonal flows? Are these neutral winds caused by storm-time Joule heating and particle precipitation that have occurred at night (and then the neutral winds have come over the poles to the dayside) or is this due to dayside storm-time heating [*Tsurutani et al.*, 2001]? Is the storm intensity a large factor in this effect, i.e., does the precipitation at lower magnetic latitudes enhance this effect greatly?

## 7.  Final Comments

[56]  The dayside and nightside ionospheric responses to the imposed interplanetary electric field and concomitant magnetic storm were in some ways similar and other ways dissimilar to each other. Although it seems apparent that both hemispheres experience a >2 hour prompt penetrating electric field (eastward on the dayside and westward at night), the dayside ionospheric uplift lasted longer than the westward electric fields at night. One possible explanation is the dissimilar nature of the ionosphere during day from night. The higher ionospheric conductivity during day may lead to considerably longer shielding time scale in this region [*Southwood*, 1977; *Southwood and Wolf*, 1978].

[57]  We find that the interplanetary electric field has an enormous effect on the dayside ionosphere. We are only beginning to understand the full ramifications.

## References

Abdu, M. A. (1997), Major phenomena of the equatorial ionosphere-thermosphere system under disturbed conditions, *J. Atmos. Sol. Terr. Phys.*, *59*, 1505.

Abdu, M. A., I. S. Batista, G. O. Walker, J. H. A. Sobral, N. B. Trivedi, and E. R. de Paula (1995), Equatorial ionospheric electric field during magnetospheric disturbances: Local time/longitude dependences from recent EITS campaigns, *J. Atmos. Terr. Phys.*, *57*, 1065.

Abdu, M. A., J. H. Sastri, J. MacDougall, I. S. Batista, and J. H. A. Sobral (1997), Equatorial disturbance dynamo electric field, longitudinal structure and spread-F: A case study from GUARA/EITS campaigns, *Geophys. Res. Lett.*, *24*, 1707.

Abdu, M. A., I. S. Batista, H. Takahashi, J. MacDougall, J. H. Sobral, A. F. Medeiros, and N. B. Trivedi (2003), Magnetospheric disturbance induced equatorial plasma bubble development and dynamics: A case study in Brazilian sector, *J. Geophys. Res.*, *108*(A12), 1449, doi:10.1029/2002JA009721.

Batista, I. S., E. R. de Paula, M. A. Abdu, and N. B. Trivedi (1991), Ionospheric effects of the 13 March 1989 magnetic storm at low latitudes, *J. Geophys. Res.*, *96*, 13,943.

Bittencourt, J. A., and M. A. Abdu (1981), A theoretical comparison between apparent and real vertical ionization drift velocities in the equatorial F region, *J. Geophys. Res.*, *86*, 2451.

Blanc, M., and A. D. Richmond (1980), The ionospheric disturbance dynamo, *J. Geophys. Res.*, *85*, 1669.

Buonsanto, M. J. (1999), Ionospheric storms—A review, *Space Sci. Rev.*, *88*, 563.

Fejer, B. G., and J. T. Emmert (2003), Low-latitude ionospheric disturbance electric field effects during the recovery phase of the 19–21 October 1998 magnetic storm, *J. Geophys. Res.*, *108*(A12), 1454, doi:10.1029/2003JA010190.

Fejer, B. G., and L. Scherliess (1995), Time dependent response of equatorial ionospheric electric fields to magnetospheric disturbances, *Geophys. Res. Lett.*, *22*, 851.

Fejer, B. G., R. W. Spiro, R. A. Wolf, and J. C. Foster (1990), Latitudinal variation of perturbation electric fields during magnetically disturbed periods: 1986 SUNDIAL observations and model results, *Ann. Geophys.*, *8*, 441.

Foster, J. C., and H. B. Vo (2002), Average characteristics and activity dependence of the subauroral polarization stream, *J. Geophys. Res.*, *107*(A12), 1475, doi:10.1029/2002JA009409.

Foster, J. C., P. J. Erickson, A. J. Coster, J. Goldstein, and F. J. Rich (2002), Ionospheric signatures of plasmaspheric tails, *Geophys. Res. Lett.*, *29*(13), 1623, doi:10.1029/2002GL015067.

Fuller-Rowell, T. M., M. V. Codrescu, R. G. Roble, and A. D. Richmond (1997), How does the thermosphere and ionosphere react to a geomagnetic storm?, in *Magnetic Storm, Geophys. Monogr. Ser.*, vol. 98, edited by B. T. Tsurutani et al., p. 203, AGU, Washington, D.C.

Fuller-Rowell, T. M., G. H. Millward, A. D. Richmond, and M. V. Codrescu (2002), Storm-time changes in the upper atmosphere at low latitudes, *J. Atmos. Sol. Terr. Phys.*, *64*, 1383.

Gonzalez, W. D., and B. T. Tsurutani (1987), Criteria of interplanetary parameters causing intense magnetic storms (Dst < −100 nT), *Planet. Space Sci.*, *35*, 1101.

Gonzalez, W. D., J. A. Joselyn, Y. Kamide, H. W. Kroehl, G. Rostoker, B. T. Tsurutani, and V. M. Vasyliunas (1994), What is a geomagnetic storm?, *J. Geophys. Res.*, *99*, 5771.

Kamide, Y., et al. (1998), Current understanding of magnetic storms: Storm-substorm relationships, *J. Geophys. Res.*, *103*, 17,705.

Kelley, M. C., J. J. Makela, J. L. Chau, and M. J. Nicolls (2003), Penetration of the solar wind electric field into the magnetosphere/ionosphere system, *Geophys. Res. Lett.*, *30*(4), 1158, doi:10.1029/2002GL016321.

Klein, L. W., and L. F. Burlaga (1982), Inter-planetary magnetic clouds at 1-AU, *J. Geophys. Res.*, *87*, 613.

Kozyra, J. U., V. K. Jordanova, R. B. Horne, and R. M. Thorne (1997), Modeling the contribution of the electromagnetic ion cyclotron (EMIC) waves to stormtime ring current erosion, in *Magnetic Storms, Geophys. Monogr. Ser.*, vol. 98, edited by B. T. Tsurutani et al., pp. 187–202, AGU, Washington, D. C.

Lu, G., A. D. Richmond, R. G. Roble, and B. A. Emery (2001), Coexistence of ionospheric positive and negative storm phases under northern winter conditions: A case study, *J. Geophys. Res.*, *106*, 24,493.

Mannucci, A. J., B. D. Wilson, D. N. Yuan, C. M. Ho, U. J. Lindqwister, and T. F. Runge (1998), A global mapping technique for GPS-derived ionospheric total electron content measurements, *Radio Sci.*, *33*, 565.

McComas, D. J., S. J. Bame, P. Barker, W. C. Feldman, J. L. Phillips, P. Riley, and J. W. Griffee (1998), Solar wind electron proton alpha monitor (SWEPAM) for the Advanced Composition Explorer, *Space Sci. Rev.*, *86*, 563.

Proelss, G. W. (1997), Magnetic storm associated perturbations of the upper atmosphere, in *Magnetic Storms, Geophys. Monogr. Ser.*, vol. 98, edited by B. T. Tsurutani et al., p. 227–241, AGU, Washington, D.C.

Reinisch, B. W., X. Huang, P. Song, J. L. Green, S. F. Fung, V. M. Vasyliunas, D. L. Gallagher, and B. R. Sandel (2004), Plasmaspheric

mass loss and refilling as a result of a magnetic storm, *J. Geophys. Res.*, *109*, A01202, doi:10.1029/2003JA009948.

Richmond, A. D., and G. Lu (2000), Upper-atmospheric effects of magnetic storms: A brief tutorial, *J. Atmos. Sol. Terr. Phys.*, *62*, 1115.

Sastri, J. H. (1988), Equatorial electric fields of the disturbance dynamo origin, *Ann. Geophys.*, *6*, 635.

Sastri, J. H., K. Niranjan, and K. S. V. Subbarao (2002), Response of the equatorial ionosphere in the Indian (midnight) sector to the severe magnetic storm of July 15, 2000, *Geophys. Res. Lett.*, *29*(13), 1651, doi:10.1029/2002GL015133.

Scherliess, L., and B. G. Fejer (1997), Storm time dependence of equatorial disturbance dynamo zonal electric field, *J. Geophys. Res.*, *102*, 24,037.

Senior, C., and M. Blanc (1984), On the control of magnetospheric convection by the spatial distribution of ionospheric conductivities, *J. Geophys. Res.*, *89*, 261.

Smith, C. W., M. H. Acuna, L. F. Burlaga, J. L'Heureux, N. F. Ness, and J. Scheifele (1998), The ACE magnetic field experiment, *Space Sci. Rev.*, *86*, 613.

Sobral, J. H. A., M. A. Abdu, W. D. Gonzalez, I. Batista, and A. L. Clua de Gonzalez (1997), Low-latitude ionospheric response during intense magnetic storms at solar maximum, *J. Geophys. Res.*, *102*, 14,305.

Sobral, J. H. A., M. A. Abdu, W. D. Gonzalez, C. S. Yamashita, A. L. Clua de Gonzalez, I. Batista, and C. J. Zamlutti (2001), Responses of the low latitude ionosphere to very intense geomagnetic storms, *J. Atmos. Sol. Terr. Phys.*, *63*, 965.

Southwood, D. J. (1977), Role of hot plasma in magnetospheric convection, *J. Geophys. Res.*, *82*, 5512.

Southwood, D. J., and R. A. Wolf (1978), Assessment of roles of precipitation in magnetospheric convection, *J. Geophys. Res.*, *83*, 5227.

Spiro, R. W., R. A. Wolf, and B. G. Fejer (1988), Penetration of high latitude electric field effects to low latitudes during SUNDIAL 1984, *Ann. Geophys.*, *6*, 39.

Tanaka, T., and K. Hirao (1973), Effects of an electric field on the dynamical behavior of the ionospheres and its application to the storm time disturbances of the F-layer, *J. Atmos. Terr. Phys.*, *35*, 1443.

Tsurutani, B. T., and W. D. Gonzalez (1997), The interplanetary causes of magnetic storms: A review, in *Magnetic Storms*, *Geophys. Monogr. Ser.*, vol. 98, edited by B. T. Tsurutani et al., pp. 77–89, AGU, Washington, D. C.

Tsurutani, B. T., and X. Y. Zhou (2003), Interplanetary shock triggering of substorms: WIND and POLAR, *Adv. Space Res.*, *31*, 1063.

Tsurutani, B. T., W. D. Gonzalez, F. Tang, S. I. Akasofu, and E. J. Smith (1988), Origin of interplanetary southward magnetic fields responsible for major magnetic storms near solar maximum (1978–1979), *J. Geophys. Res.*, *93*, 8519.

Tsurutani, B. T., et al. (2001), Auroral zone dayside precipitation during magnetic storm initial phases, *J. Atmos. Sol. Terr. Phys.*, *63*, 513.

Tsurutani, B. T., W. D. Gonzalez, X.-Y. Zhou, R. P. Lepping, and V. Bothmer (2004), Properties of slow magnetic clouds, *J. Atmos. Sol. Terr. Phys.*, *66*, 147.

Zhou, X. Y., and B. T. Tsurutani (2001), Interplanetary shock triggering of nightside geomagnetic activity: Substorms, pseudobreakups, and quiescent events, *J. Geophys. Res.*, *106*, 18,957.

————————

M. A. Abdu, W. Gonzalez, F. Guarnieri, and J. H. A. Sobral, Instituto Nacional de Pesquisas Espaciais, CP 515, 12245-970, São José dos Campos, São Paulo, Brazil. (abdu@dae.inpe.br; gonzalez@dge.inpe.br; guarnier@dge.inpe.br; sobral@dae.inpe.br)

A. Coster and J. C. Foster, Haystack Observatory, Massachusetts Institute of Technology, Westford, MA 01886, USA. (ajc@haystack.mit.edu; jcf@haystack.mit.edu)

B. Fejer, Center for Atmospheric and Space Science, Utah State University, UMC 4405, Logan, UT 84322-4405, USA. (bfejer@cc.usu.edu)

T. J. Fuller-Rowell, Space Environment Center, R/SEC, 325 Broadway, Boulder, CO 80305-3328, USA. (tim.fuller-rowell@noaa.gov)

B. Iijima, A. Mannucci, and B. Tsurutani, Jet Propulsion Laboratory, 4800 Oak Grove Dr., Pasadena, CA 91109, USA. (byron.iijima@jpl.nasa.gov; anthony.mannucci@jpl.nasa.gov; bruce.tsurutani@jpl.nasa.gov)

J. Kozyra, Department of Atmospheric, Oceanic, and Space Sciences, University of Michigan, 1414 Space Research Building, Ann Arbor, MI 48109-2143, USA.

A. Saito, Department of Geophysics, Kyoto University, Kyoto 606-8502, Japan. (saitoua@kugi.kyoto-u.ac.jp)

T. Tsuda, Research Institute for Sustainable Humanosphere, Kyoto University, Gokasho, Uji, Kyoto 611-0011, Japan. (tsuda@kurasc.kyoto-u.ac.jp)

V. M. Vasyliunas, Max-Planck-Institut für Sonnensystemforschung, 37191 Katlenburg-Lindau, Germany. (vasyliunas@linmpi.mpg.de)

K. Yumoto, Space Environment Research Center, Kyushu University, 6-10-1 Hakozaki, Fukuoka 812-8581, Japan. (yumoto@serc.kyushu-u.ac.jp)